IET Electric Power Applications

Research Article

IET Journals
The Institution of Engineering and Technology

Simultaneous radial deformation and partial discharge detection of high-voltage winding of power transformer

ISSN 1751-8660
Received on 23rd June 2019
Revised 17th October 2019
Accepted on 26th November 2019
E-First on 30th January 2020
doi: 10.1049/iet-epa.2019.0528
www.ietdl.org

Hossein Karami[1] ✉, Gevork B. Gharehpetian[1], Yaser Norouzi[1], Maryam Akhavan-Hejazi[2]

[1]*Department of Electrical Engineering, Amirkabir University of Technology, Iran*
[2]*Department of Electrical Engineering, University of Kashan, Iran*
✉ *E-mail: h.karami@aut.ac.ir*

Abstract: Condition monitoring of power transformers has attracted a lot of attention due to their important roles in determining power system reliability. Radial deformation of power transformer winding should be monitored online to prevent more damages to winding and possible transformer outage. The ultra-high-frequency (UHF) stepped-frequency synthetic-aperture radar imaging method has recently been proposed as an online method for high-voltage winding radial deformation detection. On the other hand, partial discharge (PD) as another defect of the transformer winding propagates UHF signals in the transformer environment, which should be detected online. In this study, the practical application of a designed monitoring system is investigated for simultaneous online detection of both PD and radial deformation defects in a real three-phase power transformer. In addition, radial deformation is localised through a monitoring system designed based on the proposed method. Using this system, only one set of antennas is needed to detect both defects which lead to reducing the number of installed antennas and economic application of the monitoring system.

Nomenclature

Variables

$ae^{j\theta}$	transmitted signal
c	wave speed
d_M	distance between two neighbouring measured positions
d_0	special position (point)
$f(.)$	boundary field value
f_l	lowest frequency
f_u	highest frequency
l	index of the measured position of antennas on the Y-axis
L	total number of measured positions
M	number of image pixels on the Y-axes
N	number of image pixels on the X-axes
N_f	number of frequency steps
N_{FFT}	number of fast Fourier transform (FFT) bins
P_{fa}	probability of false alarm
r_n	nth FFT bin of received signal
T_s	scanning sampling time
η	threshold value for partial discharge (PD) detection during synthetic aperture radar imaging procedure
σ_0^2	variance of background noise
σ_1^2	variance of PD signal
Δf	frequency step

1 Introduction

The reliability of power networks is enhanced by the online monitoring of important and expensive equipment [1, 2]. One equipment is the power transformer, and its outage may lead to large blackouts [3, 4]. Partial discharge (PD) and radial deformation (RD) of transformer winding are two major defects of this device that should be detected in early stages to prevent defect extension and transformer unavailability [5, 6]. This problem can be solved by online detection methods. The electromagnetic-based approach, described in the study, is one of the recent and proper solutions for online detection of these defects. In the following, a brief review of previous works for the detection of both defects using electromagnetic waves is provided.

1.1 RD detection of transformer winding

Some events such as short circuits and unsuitable transportation can cause winding RD. There are several methods for detection of this defect such as transfer function [7], ultra-wideband (UWB) sensor-based [8, 9] and hyperboloid methods [10, 11], some of which are still under study and development. One of the drawbacks of previous works is that most of them cannot localise defects online such as the frequency response analysis method which the effects of grid and load have not been solved for online application. However, some standards have been introduced for offline application of these methods [12]. Another drawback of some previous methods is that they need a database about the effects of different defects on the results of the method before applying it [8, 9]. In other words, different RDs should be applied on a winding and the results should be recorded and applied to a classifier to be saved as a database. Then, if a defect occurs in the same winding, the comparison of the results with a database can help to detect the defect.

Recently, the synthetic aperture radar (SAR) imaging as a novel online method has been proposed and investigated [13, 14]. In this method, there is no need to have information about RD effects before applying the method. In the previous studies, a short UWB Gaussian wave is sent in the frequency range of 3–6 GHz. The received signal reflected from the winding gives one-dimensional (1D) information about the winding. In order to have 2D information, the position of antennas along the height of the winding is changed. An image is generated using the Kirchhoff's migration method (KMM) as described in [13, 14] and the proposed method is based on comparison of the generated image in the sound condition of the transformer with the image of the transformer in future states to detect deformation if there is any difference in images. The main advantage of this method compared with the Frequency Response Analysis (FRA) method is that the SAR imaging method can be used online and the grid or load does not have any effect on the results.

1.2 PD detection

PD affects dielectric and insulation of electrical equipment and its detection in its early stage is very important [15–17]. Online

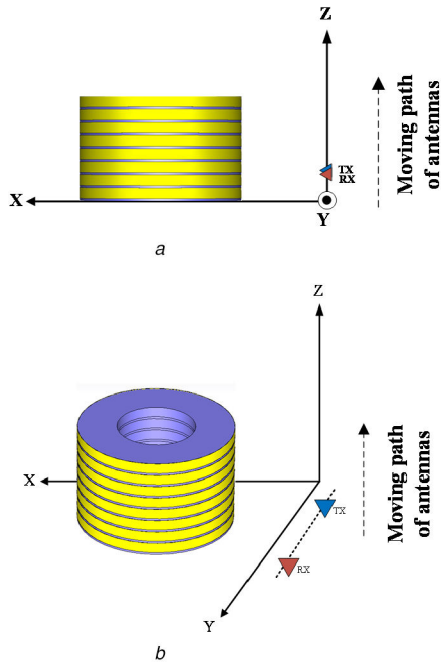

Fig. 1 *Moving path of antennas in SAR imaging method*
(a) *X–Z* side view, ***(b)*** 3D view

detection can show the extension of PD and so, the possibility of an outage of the transformer. A PD source propagates ultra-high-frequency (UHF) electromagnetic waves in the transformer environment in the range of 0.3–3 GHz. The emitted signal can be received by UHF antennas [18]. Installing UHF antennas and detecting PDs in transformers have been studied using simulations [19] and the applicability of this method in a real transformer has been investigated in previous research studies such as [20].

1.3 Simultaneous detection of RD and PD defects

Some of the RD defects may lead to PD defects in the transformer and so, simultaneous occurrence maybe seen. This is due to this fact that winding RD can lead to a decrease in the distance between the winding and pressboard barrier and so, the occurrence of PD [21]. Therefore, simultaneous detection of RD and PD is important, especially where each of them may affect the detection of another defect. There are not many papers on this issue. As mentioned, PD and RD defects can be detected using electromagnetic antennas. In [22], through a simulation in CST software, SAR imaging has been proposed in the UHF band to use only one set of UHF antennas to detect PD and RD defects. However, it has been shown that detection of both defects using the same band of frequency, causes corrupted generated images due to the occurrence of PD during the SAR imaging procedure. In this condition, it is possible to make the wrong decision about the condition of the winding, because the received signal is the non-separable sum of the reflected Gaussian wave from the winding and PD signal. Therefore, it is not possible to say that the variation in the received signal is due to RD or PD occurrence. To solve this problem, the stepped frequency (SF) SAR imaging approach has been proposed and the PD effect on RD detection results has been eliminated using the generalised likelihood ratio test [22]. In the SF SAR imaging method, sinusoidal waves are transmitted step by step instead of transmitting a Gaussian wave, and so, the final reflected signal from the winding can be achieved by summing the received waves. However, the previous research studies were based on simulations and practical studies have not been investigated. In addition, the simultaneous detection of both defects has not been investigated. In [23], according to the approach proposed in [22], the design of a monitoring system has been carried out to detect both defects using one set of antennas. The system has been tested on a single-phase transformer winding and the results of detection of both defects were acceptable. However, the designed monitoring system has not been investigated for a real three-phase transformer considering its complete structure such as oil, core, and tank. In addition, the simultaneous detection of both defects and localisation of RD defect using the UHF SF SAR imaging method has not been investigated in previous research studies.

In this study, the monitoring system is applied to three-phase transformer winding, where the structure of the transformer is considered including its core, tank, and oil. Since the transformer tank is like a shield versus electromagnetic waves, a dielectric window is implemented on one side of the transformer tank to make possible the transmission and reception of electromagnetic signals.

At first, the RD is detected in PD-free conditions. Then, the PD effect on the received signals is shown and the simultaneous detection of both PD and RD defects is discussed. The results of this study not only show the applicability of using a dielectric window for RD detection of high-voltage (HV) winding through the UHF SF SAR imaging method but also the results indicate the feasibility of the simultaneous detection of RD and PD defects on the real three-phase transformer. In addition, the localisation of the RD defect using the UHF SF SAR imaging method is investigated.

The novelties of the study can be summarised as follows:

- Applicability of using a dielectric window for RD detection of HV winding through the UHF SF SAR imaging method.
- Applying simultaneous detection of RD and PD defects on a real three-phase transformer.
- Localisation of RD defect using the UHF SF SAR imaging method on the real three-phase transformer.

The rest of the paper is organised as follows:

In Section 2, a brief description of applying SAR imaging to the transformer winding and SF approach are explained. In Section 3, the design of the monitoring system is stated. After that, the detection of PD and RD on a single-phase winding is discussed and then, a dielectric window is implemented on a three-phase transformer tank to investigate the performance of the monitoring system in real transformer for simultaneous detection of PD and RD, in addition to localisation of RD. Finally, the paper is concluded in Section 5.

2 Proposed defects detection method

2.1 SAR imaging method for RD detection

Fig. 1 shows a schematic of the SAR imaging set-up. In this method, a Gaussian pulse from the transmitting antenna is sent and the receiving (RX) antenna records the reflected signal from the winding. The reflected signal from the winding gives 1D information about it. In order to obtain 2D information, the antennas are moved along the moving path shown in Fig. 1 and the procedure of sending and RX of the signals is repeated in each position of antennas.

The received signals need some data processing before using them. The transmitted signals propagate in the environment and the received signals have some information from unwanted parts of the transformer such as a tank. The unwanted parts can be eliminated by determining the shortest and longest propagation paths of signal from the transmitting antenna to the RX one. Then, the RX time of the signal to the RX is calculated for each path and so, the longest time and shortest time of the signal, which have useful information about the winding, can be calculated.

After the pre-processing step, the KMM is applied to the signals and a 2D image of the winding is generated. In KMM, as formulated by (1), the magnitude of the reflected signals at each location of antennas is calculated. The details of KMM and image generation have been described in [22]. The schematic of applying KMM is shown in Fig. 2

$$U(id_0, jd_0) = \frac{d_M \cdot jd_0}{2\pi \cdot R^2 \cdot \nu \cdot T_s} \times \sum_l [f(ld_M, (n+1)T_s) - f(ld_M, nT_s)]\Big|_{nT_s = 2R/\nu} \quad (1)$$

$$i, j, l \in Z \text{ and } 1 \le l < L,\ 0 \le j < N,\ 0 \le i < M$$

$U(id_0, jd_0)$ shows the wave reflection at the pixel $(x, z) = (id_0, jd_0)$.

This is the summation of the wave reflection for all the measuring positions at each pixel. Fig. 2 shows one arbitrary position of antennas and the observation pixel. Each scan of winding can be assumed as its finger print. In other words, by comparison of generated images in sound and deformed conditions, the RD can be detected. It means that when there is no deformation and the transformer is in the manufacturing lab or starting stage of operation, the radar imaging is carried out and an image of winding is generated. This image is named as a reference image. After the operation of the transformer for a period of time, which is dependent on the transformer owner, the radar imaging is repeated and a new image is generated. If the new image is similar to the reference image, it can be concluded that there is no deformation in the HV winding. However, in case of any difference, it can be said that deformation has occurred in the HV winding. In order to quantitatively compare the images, as described in [22, 23], each colour of the generated image is defined by a number between 0 and 1. For example, number 0.4 can be selected to separate colours into two groups: cold and warm colours [22, 23]. By comparison of the number of warm colours (NWC) in images, the RD can be detected. It should be noted that as discussed in [14, 22], this approach can only detect RD in HV winding and it cannot detect low-voltage RD.

The mentioned approach for RD detection in the UHF band has acceptable results if there is no PD in the transformer. The occurrence of a PD during the SAR imaging procedure leads to adding a PD signal to the reflected Gaussian signal from the winding. Therefore, the generated image will be different in comparison with the reference image even in sound condition. In other words, the SAR imaging cannot distinguish that the differences are due to an RD or PD occurrence. Therefore, it can lead to a wrong decision. Details of this issue have been discussed in [22]. To solve this issue, SF SAR imaging has been proposed.

2.2 SF SAR imaging

SAR imaging can be implemented through two techniques: a frequency-domain technique by sending SF waves [22, 23] or a time-domain technique by sending a Gaussian wave [13, 24]. The first one is based on Fourier series, i.e. a range of sinusoidal signals can be sent and received, instead of using a Gaussian pulse. In other words, at each location of antennas, a sinusoidal signal is swept from f_l to f_u, where $N_f = (f_u - f_l)/\Delta f$. This means that at each location, at first a sinusoidal wave with the frequency of f_l is transmitted by the radar and its reflection from the object is recorded. When it can be confirmed that sufficient time is passed and the reflected wave from the object is received, another sinusoidal wave, which has a frequency of $(f_l + \Delta f)$, is transmitted to the object. Since the frequency of the transmitted sinusoidal wave is lower than f_u, this procedure of sending and RX is repeated otherwise the procedure for this location is finished and the amplitude and phase of the received signals are calculated. A time-domain signal is prepared by using an inverse FFT of them. Then, the location of antennas should be changed to the next predetermined location and the procedure should be repeated. Finally, by using KMM, the winding image is generated.

2.3 PD detection during SF SAR imaging

In the SF SAR imaging method, after transmitting each sinusoidal signal, the received signal is a sinusoidal signal with the same frequency but different amplitude and phase [22]. In other words, only the magnitude and phase of the transmitted signal are different from the received signal. This statement is true if there is no PD in the transformer environment. The PD, due to its wide range of frequency content in the UHF band, leads to the appearance of other frequencies in addition to the transmitted frequency in the received signal and so, the SAR imaging result is unreliable because the received signal is not a PD-free signal. In this situation, since a PD-free signal is achieved, the procedure of TX and RX sinusoidal signals in that frequency should be repeated. About the possibility of achieving a PD-free signal, it should be noted that, on the one hand, the time duration from sending a sinusoidal signal and RX the reflected one is <5 ns considering that the distance between antennas and winding is <40 cm. On the other hand, there can be <10 PD pulses per AC half cycle in power transformers [25]. It means that the time duration between two successive PD occurrences is >100 ns, which compared with 5 ns means that achieving a PD-free signal is possible.

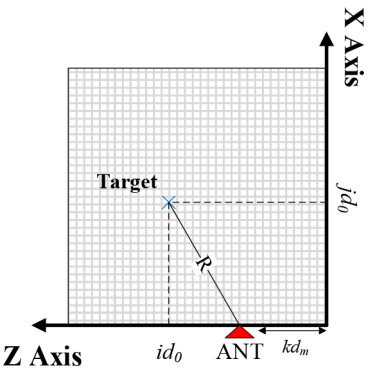

Fig. 2 *Schematic of applying KMM according to (1)*

One important point in this step is that there is no need to repeat the SF SAR imaging procedure for all frequencies if a PD occurs during the procedure. It is enough to repeat the procedure only at the frequency/frequencies in which the PD has occurred.

In order to make the correct decision about the PD occurrence, the fast Fourier transform (FFT) of the received signal should be investigated. In PD-free conditions, as discussed in [22], in the received signal there is a sinusoidal signal, which frequency is known but its amplitude and phase are unknown, combined with the noise of the environment. It means that except for a peak at the frequency of the transmitted signal, there is noise in all bins of FFT of the signal. After PD occurrence during the SF SAR imaging procedure, because of the wide frequency content of PD signal, not only there is a peak at the transmitted frequency, but also other bins have a higher level than background noise.

According to the detection theory, in the null hypothesis (H_0), there is no PD and so, at the kth bin, there is transmitted signal content in the FFT of signal and others should be background noise. The probability density functions (PDFs) of FFT bins under the null hypothesis can be represented as follows:

$$f(r_k|H_0) = \frac{1}{\sigma_0\sqrt{2\pi}}\exp\left(-\frac{|r_k - ae^{j\theta}|^2}{2\sigma_0^2}\right) \quad (2)$$

$$f(r_n|H_0) = \frac{1}{\sigma_0\sqrt{2\pi}}\exp\left(-\frac{|r_n|^2}{2\sigma_0^2}\right),\ n = 1, 2, \ldots, N_{FFT}, n \ne k \quad (3)$$

On the alternative hypothesis (H_1), it is assumed that the PD occurrence has happened. The PDFs of FFT bins can be written as follows:

$$f(r_k|H_1) = \frac{1}{\sqrt{2\pi(\sigma_0^2 + \sigma_1^2)}}\exp\left(-\frac{|r_k - ae^{j\theta}|^2}{2(\sigma_0^2 + \sigma_1^2)}\right) \quad (4)$$

$$f(r_n|H_1) = \frac{1}{\sqrt{2\pi(\sigma_0^2 + \sigma_1^2)}}\exp\left(-\frac{|r_n|^2}{2(\sigma_0^2 + \sigma_1^2)}\right) \quad (5)$$

$$n = 1, 2, \ldots, N_{FFT},\ n \ne k$$

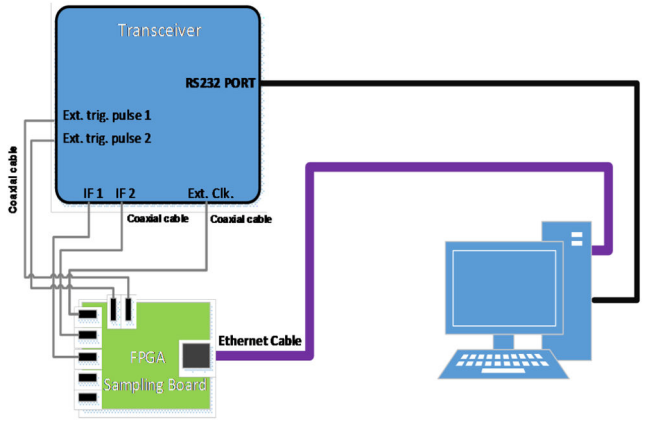

Fig. 3 *Designed a monitoring system for the detection of RD and PD*

Considering the maximum likelihood method and Neyman–Pearson lemma, according to the generalised likelihood ratio test, the decision of PD occurrence can be made using the following inequality [22]:

$$\sum_{n=1, n\neq k}^{N_{\mathrm{FFT}}} |r_n|^2 \underset{H_1}{\overset{H_0}{\lessgtr}} \eta \tag{6}$$

The formulation of the right-hand side of (6) has been described in [22]. This value is calculated in the sound condition of the transformer according to σ_0^2 and σ_1^2 [22]. Then during SAR imaging and in each frequency step of transmitting and RX signals, the left-hand side of (6) should be calculated and compared with the threshold according to (6) for detection of possible PD occurrence during SAR imaging. If the PD occurrence is detected during the procedure of SAR imaging at a frequency step, the procedure of TX and RX signals in that frequency should be repeated until RX a PD-free signal. Using the mentioned theory, a monitoring system is designed which will be described in Section 3.

2.4 PD detection in a passive mode of the monitoring system

As mentioned before, the PD signal has a wide-band frequency range due to its characteristics. This specification can help to detect PD. When the monitoring system is working in passive mode and the transformer is in sound condition without any PD, a signal should be recorded to evaluate the noise level of the environment of the inside of the transformer as the reference threshold. Then, if during the operation of the transformer, a wide-band signal in which its amplitude is higher than the reference noise level is received, it can be concluded that a PD has occurred. In order to numerically show the PD detection, similar to the discussion in the previous subsection, the summation of FFT bins of the reference environment noise signal should be calculated, which can be formulated as follows:

$$\mathrm{PDTh} = \sum_{n=1}^{N} |r_n|^2 \tag{7}$$

During the operation of the transformer, the value of the right-hand side of (7) is calculated while the monitoring system is in passive mode and if its value is higher than the threshold for PD detection (PDTh), it can be concluded that a PD has occurred. Section 4 will show the experimental results of PD detection.

It should be noted that the propagation of PD occurred inside the transformer winding leads to a decrease in the amplitude of UHF electromagnetic waves. However, as discussed in [24], the decrease of the PD amplitude is about 18 dB and detection of PD >500 pC is possible using antennas installed on the internal wall of the tank.

2.5 Procedure for arbitrary transformer

In this subsection, the procedure of detection of RD and PD is described for arbitrary transformer step by step. The procedure has 14 steps in two main stages in which each stage has two sub-stages as follows:

Stage 1: initial procedure in sound (reference) condition

Stage 1-1: reference threshold for RD detection

Step 1: place the RX and TX antennas in the first scanning position (point) at the same height with the bottom of the transformer winding.

Step 2: transmit a sinusoidal signal with the frequency of f_{l} and receive the reflected signal.

Step 3: increase the frequency of the signal with the step of Δf and repeat step 2 until reaching the frequency of f_{u}.

Step 4: change the position of antennas to the next scanning position and repeat steps 2 and 3 until reaching the Lth position (final scanning position), which is at the same height with the top of the transformer winding.

Step 5: generate an image by applying (1) on the received signals.

Step 6: calculate NWC in the generated image to be used as the threshold of RD detection.

Stage 1-2: reference thresholds for PD detection

Step 7: record the signals from the RX antennas when the monitoring system is in the passive mode.

Step 8: calculate the noise level as the PDTh according to (7).

Step 9: calculate the threshold of PD detection during the SAR imaging procedure according to (6). This is the value of the right-hand side of (6). This threshold will be used for PD detection during the SAR imaging procedure or simultaneous PD and RD detection.

Stage 2: evaluation of future states of transformer

Stage 2-1: RD detection or simultaneous RD and PD detection

Step 10: repeat Steps 1–3. In each frequency step, after RX the reflected signal, calculate the left-hand side of (6) and compare with the threshold calculated in step 9. Using (6), the occurrence of PD during the SAR imaging procedure can be detected.

Step 11: if the PD occurrence has not been detected at any frequency step, the SAR imaging procedure should be continued and step 4 should be carried out. Otherwise, if the PD occurrence has been detected while the SAR imaging procedure is at the frequency of f_0, the SAR imaging procedure should not start the next frequency step, $(f_0 + \Delta f)$. The procedure of TX and RX signals at the frequency of f_0 should be repeated until achieving a PD-free signal as described in Section 2.3. After RX a PD-free signal for the frequency step of f_0, SAR imaging for the next frequency steps should be continued.

Step 12: repeat step 5 to generate images based on new data and calculate NWC in the newly generated image.

Step 13: compare the NWC of a new image with NWC of the reference image calculated in step 6 as the threshold. If it is greater than the threshold, RD has occurred.

Stage 2-2: PD detection

Step 14: repeat step 7 and calculate the right-hand side of (7). If it is greater than PDTh, PD has occurred.

3 Design of monitoring system

As shown in Fig. 3, the transceiver and sampling board are two main parts of the designed monitoring system. The transceiver has three parts: local oscillator, receiver, and transmitter. There are two operation modes in the system: active and passive modes. In the active mode, the RD defect is detected. If the aim is only PD detection, the passive mode is used. The frequency of the transmission section can start from 0.8 up to 3 GHz which is tuned

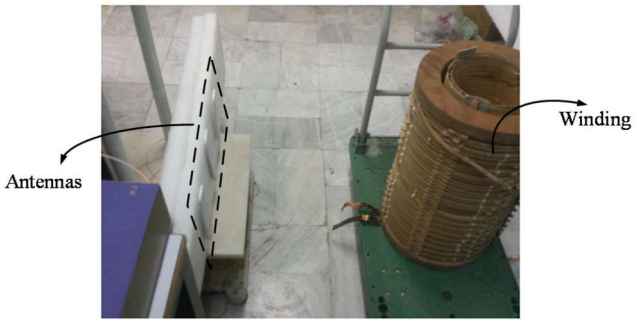

Fig. 4 *Schematic of single-phase winding and antennas*

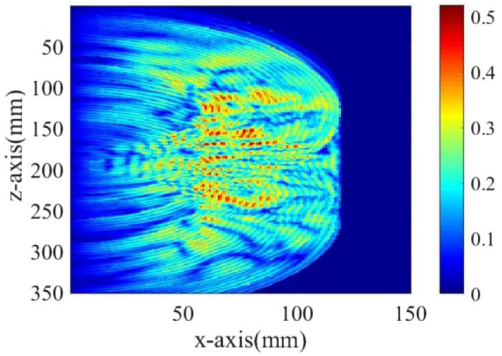

Fig. 5 *Image of single-phase winding in sound condition using UHF SF SAR method*

with 10 MHz steps. In the receiver section, if the monitoring system is in the passive mode, the frequency can receive signals from 0.1 up to 3 GHz, while in active mode can start from 0.8 up to 3 GHz. In other words, the frequency of 0.8 up to 3 GHz is common in both modes. By a graphical user interface, some parameters of the monitoring system such as lower and upper frequencies of the SF approach or power of the transmitted signal can be determined by the user. According to the parameters defined by the user, control commands are sent by the software part in the desktop computer through RS232 port. After that, using external trigger pulses, the intermediate frequency signals are sampled by a field programmable gate array. The sampled values are sent to the desktop computer to be used by KMM.

The transceiver is off in the passive mode, and only the environment signals are received. In the active mode, all parts of the transceiver are active and the power of the transmitted signal can be determined from 0 to 10 dB.

4 Experimental studies and results

In this section, the designed monitoring system is implemented on a single-phase winding and a three-phase transformer for simultaneous detection of RD and PD defects. In each case, after investigating the detection of each defect using the designed monitoring system, the simultaneous detection is also shown. In addition, in the case of a three-phase transformer, the RD localisation using the UHF SF SAR imaging method is investigated. In the active mode, the parameters of the monitoring system are $N_f = 220$, $f_u = 3$ GHz and $f_l = 0.8$ GHz.

4.1 Single-phase winding

The results of testing the designed monitoring system on a single-phase winding, which does not have any tank, dielectric window, oil, and core, are shown in this subsection. The detailed specifications of this winding are shown in Fig. 4 and the specifications of UHF antennas can be found in [14, 26], respectively. The distance between the winding and the antennas is about 70 cm.

4.1.1 Detection of RD: The UHF SF SAR imaging is performed at 16 predetermined positions alongside the height of the transformer winding in sound and deformed PD-free conditions. In the deformed condition, an RD is applied on a part of winding and using KMM, the images are generated as shown in Figs. 5 and 6.

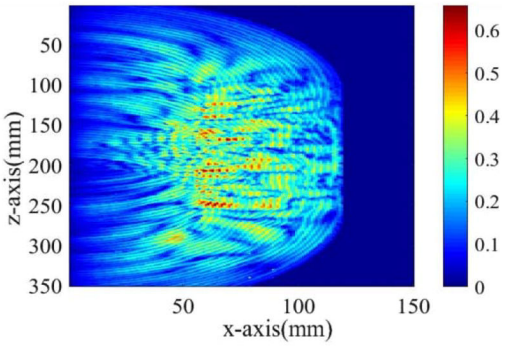

Fig. 6 *Image of single-phase winding in deformed condition using UHF SF SAR method*

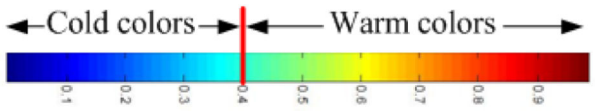

Fig. 7 *Warm and cold colours quantification*

A visual comparison of images shows that there is a deformation in the winding. In order to quantitatively compare the images, as described in [22, 23], each colour is defined by a number between 0 and 1. As can be seen in Fig. 7, number 0.4 is selected to separate cold and warm colours [22, 23, 27]. By comparison of the NWC values in the images, the RD defect can be detected. In these figures, the NWC values in deformed and sound images are 936 and 294, respectively, which indicate the occurrence of RD defect in the single-phase winding.

As the values obtained from this setup are not very high, showing these figures by defining red colour equal to 1, leads to figures which are unclear and blue colour is dominant. As can be seen from Figs. 5 and 6, in order to improve the resolution of figures, the red colour is defined equal to the maximum value in each figure. This assumption is only for depicting figures and does not affect calculating NWC. The calculation of NWC is carried out by summing the number of colour points with the colour number >0.4 for both conditions.

4.1.2 Detection of PD: The PD is generated by two needles near the winding and the monitoring system is used in the passive mode. It should be noted that all types of PD in power transformers have a wide range of frequency content and can affect SAR imaging results. All of them can be detected using electromagnetic antennas as discussed in previous papers [18–20]. In addition, the procedure of PD effect elimination from SAR imaging results is the same and can be applied for PDs with different frequency content. Therefore, investigation of one PD type can show the applicability of the monitoring system and the results of other PD types are not shown due to the similarity of the procedure.

As shown in Fig. 8*a*, in PD-free condition, there is only noise signals of environment that usually do not have significant amplitude. In the case of PD occurrence (Fig. 8*b*), the monitoring system receives signals with remarkable amplitude in a few samples which can be used to detect PD. Using (7), PDTh is set to 210 according to the noise of the environment. However, the right-hand side of (7) is about 292 in PD conditions. Therefore, it can be concluded that using the proposed method, a PD occurrence has been detected.

As the basis of the proposed method is a comparison of the current condition of the transformer with the reference (sound) condition, one is important is to use the same monitoring system with the same configuration and assumptions in both conditions. In this study, each unit of amplitude is considered 1 μV.

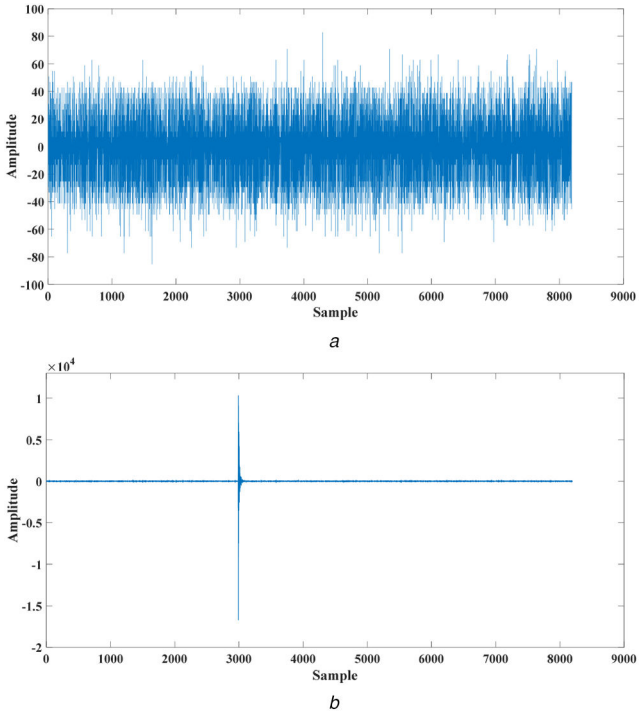

Fig. 8 *Received signal in passive mode*
(a) Noise of environment, ***(b)*** PD signal

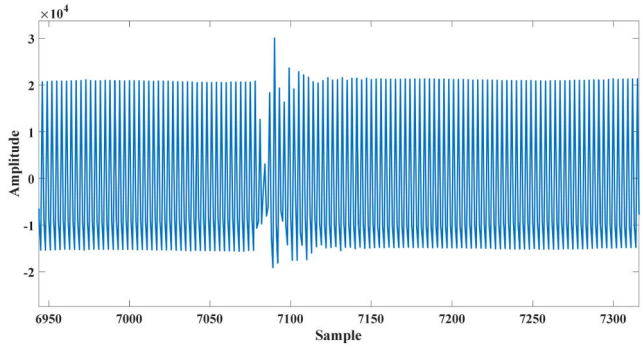

Fig. 9 *PD disturbed received signal of monitoring system in active mode*

4.1.3 Simultaneous PD and RD detection: As discussed in [22], PD occurrence during the UHF SF SAR imaging procedure can lead to corrupted generated images and so, the wrong decision about the condition of the winding, because the results of SAR imaging are unreliable. Fig. 9 shows the received signal of the SAR imaging method disturbed by a PD.

As described in Section 2.3, by comparison of the left-hand side of (6) with the threshold value, the PD occurrence is detected. The threshold value can be determined considering the environment noise when there is no PD. In this study, it is chosen equal to 310 and the left-hand side of (6) is 380 for the signal shown in Fig. 9. It means that a PD has occurred and the procedure of UHF SF SAR imaging should be repeated at that frequency to achieve a PD-free signal. Therefore, not only the PD occurrence is detected, but also its effect on UHF SF SAR imaging result is eliminated and the RD can be detected according to Section 4.1.1. It can be said that all the possible conditions of occurrence of PD and RD defects can be monitored by a designed monitoring system in the single-phase winding.

4.2 Three-phase winding

In this subsection, the applicability of the designed monitoring system on a real three-phase power transformer is tested. By using polytetrafluoroethylene, on one side of the transformer tank, a dielectric window is installed. The three-phase transformer winding outside of the tank can be seen in Fig. 10. The core and three-phase winding are inserted in the tank. After that filling the transformer tank with the transformer oil is carried out. In the active mode, the parameters of the monitoring system are $N_f = 220$, $f_u = 3$ GHz, and $f_l = 0.8$ GHz.

Fig. 10 *Setup of a three-phase transformer*

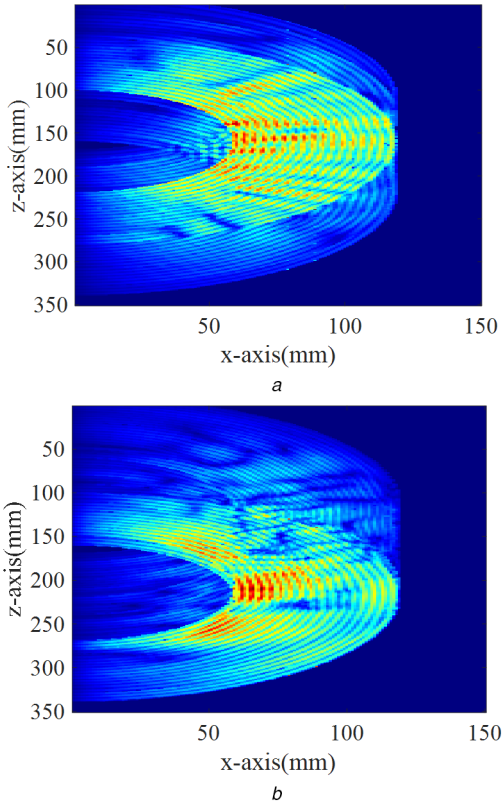

Fig. 11 *Comparison of images in three-phase winding*
(a) Image of middle winding of the three-phase transformer in sound condition using the UHF SF SAR method, ***(b)*** Image of middle winding of the three-phase transformer in deformed condition using the UHF SF SAR method

4.2.1 Detection of RD: The procedure of UHF SF SAR imaging is performed at 11 predetermined positions alongside the height of the transformer winding in sound and deformed PD-free conditions, where the distance between two adjacent positions is 3 cm. As an example, the middle winding is studied. The procedure for each winding is similar. An RD defect is applied to the top part of the middle winding. After applying KMM, the generated images are shown in Fig. 11. It can be concluded from the visual comparison that deformation has occurred in the top part of the winding due to its higher warm colours at a higher height. It should be noted that the zero point of the z-axis is in the top part of the images. The values of the NWC in sound and deformed images are 2837 and 3108, respectively, which indicate RD occurrence in the power transformer middle winding.

4.2.2 RD localisation: As described in previous sections, the procedure of UHF SF SAR imaging is carried out in L predetermined positions. The measurement at each position has an independent procedure. Therefore, the KMM can be applied on L' positions that $L' < L$. In other words, instead of generating one

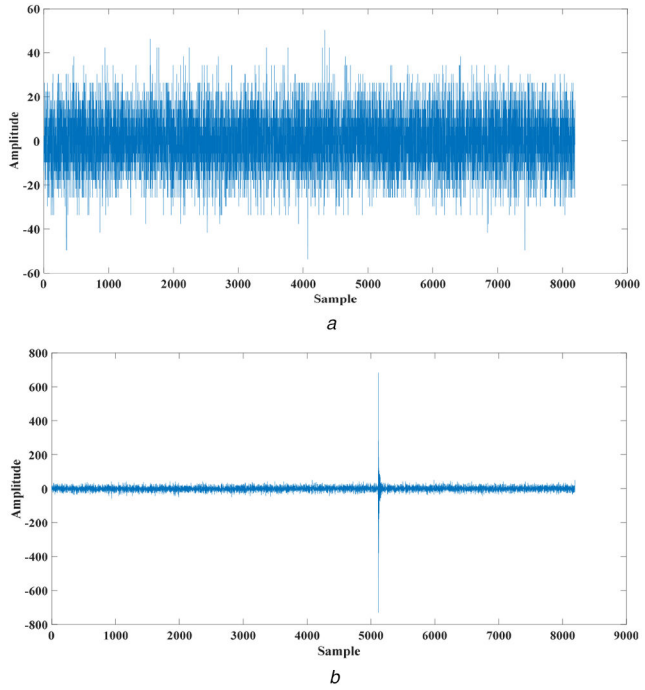

Fig. 12 *Received signal from the three-phase transformer in passive mode*
(a) Noise of environment, ***(b)*** PD signal

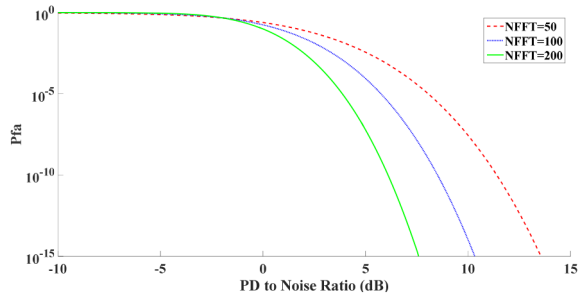

Fig. 13 *Probability of false detection variations versus noise and system parameters*

image based on scanning the whole height of the winding, the height of the winding can be divided into different parts and for measured positions of each part, the KMM is used to generate an image. Then, for sound and deformed conditions, the images of each part are compared with each other. Only the images of the deformed part of the winding have remarkable differences in the NWC values and other parts have similar NWC values in comparison to sound and deformed images. It is not necessary to have the same number of measured positions or height of scanning in different parts. For example, the height of the middle winding is divided into two parts. The top part has five measurement positions and the other one has six measurement positions. In the sound condition, the NWC values for the images of the top and bottom parts of the winding are 823 and 3109, respectively, while in the deformed condition, the NWC values are 2506 and 3148, respectively. These values show that the NWC values for the bottom part have no significant difference while in the top part, the difference is remarkable. Therefore, according to this procedure, there is an RD in the top part of the winding. This procedure can be extended by increasing the number of parts to detect the defect more accurately.

4.2.3 Detection of PD: In this transformer, PD is generated using a needle–needle electrode. The recorded noise (when there is no PD) and the captured PD signal (by the monitoring system) are shown in Figs. 12*a* and *b*, respectively. In the case of PD occurrence, the received signal has a remarkable amplitude in a few samples which can be used to detect PD. Similar to Section 4.1.2, using (7), PDTh is set to 29 according to the noise of the environment. However, the right-hand side of (7) is about 61 in PD conditions. Therefore, it can be concluded that using the proposed method, a PD occurrence has been detected. It should be noted that the propagation of PD occurred inside the transformer winding leads to a decrease in the amplitude of UHF electromagnetic waves. However, as discussed in [24], the decrease of the PD amplitude is about 18 dB and detection of PD >500 pC is possible using antennas installed on the internal wall of the tank.

4.2.4 Simultaneous PD and RD detection: Similar to the single-phase case, a threshold should be determined according to the environment condition and then, using (6), the decision should be made about the occurrence of PD during the SAR imaging procedure. In this set-up, η is selected to be equal to 45 and in a PD-polluted, the left-hand side of (6) is calculated 90, which shows the PD occurrence by numerical approach. Therefore, the procedure of UHF SF SAR imaging should be repeated at that frequency to achieve a PD-free signal. In this set-up, the simultaneous occurrence is detected to eliminate the PD effect on UHF SF SAR imaging results.

Noise level is one of the important issues in the performance of the monitoring system and it can lead to false detection. As discussed in [28], P_{fa} can be calculated according to the noise and the parameters of the system. Fig. 13 shows the variations of false detection probability versus PD to noise level and N_{FFT}.

As shown in the previous subsections, the monitoring system could detect the occurrence of PD and RD, and also their simultaneous occurrence. Moreover, the monitoring system could localise the RD alongside the winding height. By increasing the number of positions for scanning, the RD localisation could be improved.

5 Conclusion

In this study, the designed monitoring system is implemented and tested for the simultaneous detection of RD and PD on a real three-phase transformer. In addition, the applicability of using a dielectric window for RD detection of HV winding through the UHF SF SAR imaging method is investigated. Using the proposed method and the monitoring system, not only PD and RD defects are solely detected, but also the simultaneous detection is studied which has not been investigated before on a three-phase transformer. One of the most important advantages of the proposed monitoring system is that both defects are detected using only one set of UHF antennas which leads to more economic usage of this system and achieving more complete online information of transformer condition. Moreover, the RD defect is localised alongside the transformer height.

6 Acknowledgment

The first author is funded by Iran National Elites Foundation (INEF) and the second author is founded by the Iran National Science Foundation (INSF) and German Research Foundation (DFG) - project No. 38013532. The funding by INEF, DFG and INSF is greatly acknowledged.

7 References

[1] Rahbarimagham, H., Karami, H., Esmaeili, S., *et al.*: 'Determination of transformer HV winding axial displacement extent using hyperbolic method – a feasibility study', *IET Electr. Power Appl.*, 2019, **13**, (7), pp. 1004–1013
[2] Rahbarimagham, H., Karami, H., Hejazi, M.S.A., *et al.*: 'Determination of transformer winding radial deformation using UWB system and hyperboloid method', *IEEE Sens. J.*, 2015, **15**, (8), pp. 4194–4202
[3] Hernandez, H.E., Vázquez, E., Andrade, M., *et al.*: 'Extended second central moment approach to detect turn-to-turn faults in power transformers', *IET Electr. Power Appl.*, 2019, **13**, (6), pp. 773–782
[4] Patel, D., Chothani, N.G., Mistry, K.D., *et al.*: 'Design and development of fault classification algorithm based on relevance vector machine for power transformer', *IET Electr. Power Appl.*, 2018, **12**, (4), pp. 557–565
[5] Hu, E., Yang, L., Liao, R.J., *et al.*: 'Effect of an electric field on copper sulphide deposition in oil-impregnated power transformers', *IET Electr. Power Appl.*, 2016, **10**, (3), pp. 155–160
[6] Narayana, G.S., Badgujar, K.P., Kulkarni, S.V.: 'Factorisation-based transfer function estimation technique for deformation diagnostics of windings in transformers', *IET Electr. Power Appl.*, 2013, **7**, (1), pp. 39–46

[7] Ghanizadeh, A.J., Gharehpetian, G.B.: 'ANN and cross-correlation based features for discrimination between electrical and mechanical defects and their localization in transformer winding', *IEEE Trans. Dielectr. Electr. Insul.*, 2014, **21**, (5), pp. 2374–2382

[8] Hejazi, M.A., Ebrahimi, J., Gharehpetian, G.B., *et al.*: 'Application of ultra-wideband sensors for on-line monitoring of transformer winding radial deformations – a feasibility study', *IEEE Sens. J.*, 2012, **12**, (6), pp. 1649–1659

[9] Rahbarimagham, H., Esmaeili, S., Gharehpetian, G.B.: 'Discrimination between radial deformation and axial displacement in power transformers using analysis of electromagnetic waves', *IEEE Sens. J.*, 2017, **17**, (16), pp. 5324–5331

[10] Tabarsa, H., Hejazi, M.A., Gharehpetian, G.B.: 'Detection of HV winding radial deformation and PD in power transformer using stepped-frequency hyperboloid method', *IEEE Trans. Instrum. Meas.*, 2019, **68**, (8), pp. 2934–2942

[11] Rahbarimagham, H., Esmaeili, S., Gharehpetian, G.B.: 'Localization of radial deformation and its extent in power transformer HV winding using stationary UWB antennas', *IEEE Sens. J.*, 2017, **17**, (10), pp. 3184–3192

[12] 'IEEE Guide for the Application and Interpretation of Frequency Response Analysis for Oil-Immersed Transformers', IEEE Std C57.149-2012, 2013, pp. 1–72

[13] Golsorkhi, M.S., Gharepetian, G.B., Dehmollaian, M., *et al.*: 'A feasibility study on application of radar imaging for detection of transformer winding radial deformation', *IEEE Trans. Power Deliv.*, 2012, **27**, (4), pp. 2113–2121

[14] Mortazavian, S., Shabestary, M.M., Mohamed, Y.A.R.I., *et al.*: 'Experimental studies on monitoring and metering of radial deformations on transformer HV winding using image processing and UWB transceivers. Industrial informatics', *IEEE Trans.*, 2015, **11**, (6), pp. 1334–1345

[15] Yi, X., Wang, Z.: 'Creepage discharge on pressboards in synthetic and natural ester transformer liquids under ac stress', *IET Electr. Power Appl.*, 2013, **7**, (3), pp. 191–198

[16] Luo, Y., Wu, Y., Hu, J., *et al.*: 'Research on detection method for spatial discharge of high voltage electrical equipment based on ultraviolet monitoring video'. 2017 IEEE 5th Int. Symp. on Electromagnetic Compatibility (EMC-Beijing), Beijing, People's Republic of China 2017 October, pp. 1–5

[17] Tang, J., Xie, Y.: 'Partial discharge location based on time difference of energy accumulation curve of multiple signals', *IET Electr. Power Appl.*, 2011, **5**, (1), pp. 175–180

[18] Mirzaei, H.R., Akbari, A., Gockenbach, E., *et al.*: 'A novel method for ultra-high-frequency partial discharge localization in power transformers using the particle swarm optimization algorithm', *IEEE Electr. Insul. Mag.*, 2013, **29**, (2), pp. 26–39

[19] Karami, H., Hejazi, M.S.A., Naderi, M.S., *et al.*: 'Three-dimensional simulation of PD source allocation through TDOA method'. 4th Conf. on Thermal Power Plants (Gas, Combined Cycle, and Steam), Tehran, Iran, December 18-19 2012

[20] Mirzaei, H.R., Akbari, A., Gockenbach, E., *et al.*: 'Advancing new techniques for UHF PD detection and localization in the power transformers in the factory tests', *IEEE Trans. Dielectr. Electr. Insul.*, 2015, **22**, (1), pp. 448–455

[21] Sikorski, W.: 'Development of acoustic emission sensor optimized for partial discharge monitoring in power transformers', *Sensors*, 2019, **19**, (8), p. 1865

[22] Karami, H., Gharehpetian, G. B., Norouzi, Y., *et al.*: 'GLRT-based mitigation of partial discharge effect on detection of radial deformation of transformer HV winding using SAR imaging method', *IEEE Sens. J.*, 2016, **16**, (19), pp. 7234–7241

[23] Karami, H., Gharehpetian, G. B., Norouzi, Y., *et al.*: 'Experimental study on elimination of partial discharge effect on detection of radial deformation of high voltage transformer winding using electromagnetic waves'. 2018 IEEE Int. Conf. on Environment and Electrical Engineering and 2018 IEEE Industrial and Commercial Power Systems Europe (EEEIC/I&CPS Europe), Palermo, Italy, June 2018, pp. 1–5

[24] Mosayebi, R., Sheikhzadeh, H., Golsorkhi, M.S., *et al.*: 'Detection of winding radial deformation in power transformers by confocal microwave imaging', *Electr. Power Compon. Syst.*, 2014, **42**, (6), pp. 605–611

[25] Li, J., Si, W., Yao, X., *et al.*: 'Partial discharge characteristics over differently aged oil/pressboard interfaces', *IEEE Trans. Dielectr. Electr. Insul.*, 2009, **16**, (6), pp. 1640–1647

[26] Available at http://www.taoglas.com/wp-content/uploads/2015/04/TG.35.8113W.pdf

[27] Karami, H., Tabarsa, H., Gharehpetian, G. B., *et al.*: 'Feasibility study on simultaneous detection of partial discharge and axial displacement of HV transformer winding using electromagnetic waves', *IEEE Trans. Ind. Inf.*, 2019, doi: 10.1109/TII.2019.2915685

[28] Papoulis, A., Pillai, S.U.: '*Probability, random variables and stochastic processes*' (McGraw-Hill, New York, NY, USA, 2002, 4th edn.)